

Residual Reinforcement Learning for Waste-Container Lifting Using Large-Scale Cranes with Underactuated Tools

Qi Li^{†,*}, Karsten Berns[†]

[†] Robotics Research Lab, RPTU University of Kaiserslautern-Landau, Kaiserslautern, Germany

Abstract

This paper studies the container lifting phase of a waste-container recycling task in urban environments, performed by a hydraulic loader crane equipped with an underactuated discharge unit, and proposes a residual reinforcement learning (RRL) approach that combines a nominal Cartesian controller with a learned residual policy. All experiments are conducted in simulation, where the task is characterized by tight geometric tolerances between the discharge-unit hooks and the container rings relative to the overall crane scale, making precise trajectory tracking and swing suppression essential. The nominal controller uses admittance control for trajectory tracking and pendulum-aware swing damping, followed by damped least-squares inverse kinematics with a nullspace posture term to generate joint velocity commands. A PPO-trained residual policy in Isaac Lab compensates for unmodeled dynamics and parameter variations, improving precision and robustness without requiring end-to-end learning from scratch. We further employ randomized episode initialization and domain randomization over payload properties, actuator gains, and passive joint parameters to enhance generalization. Simulation results demonstrate improved tracking accuracy, reduced oscillations, and higher lifting success rates compared to the nominal controller alone.

Keywords: Robotics, Residual Reinforcement Learning, Underactuated Systems

1. Introduction

Container recycling, such as waste-glass and garbage collection, is an essential component of modern urban infrastructure. As illustrated in Fig. 1, this task is commonly performed on city streets using a truck-mounted hydraulic loader crane equipped with an underactuated discharge unit. Containers are typically located above or below ground level and are fitted with small hooking rings that must be accurately engaged to lift and empty the container into the truck. This operation is difficult because (i) cranes are typically commanded in joint space, (ii) successful hooking requires accurate TCP positioning under tight tolerances, and (iii) the underactuated discharge unit exhibits oscillations induced by crane motion. The combination of large-scale crane dynamics, underactuated tools, and small tolerance requirements makes the task physically and cognitively demanding for human operators. This difficulty is further exacerbated by the shortage of experienced operators and the high cost and time required for training, motivating the need for automation.

Automation of hydraulic machinery has received increasing attention in robotics research, with applications in construction, forestry, recycling, warehousing, and port operations [1–3]. While prior work has addressed material handling and lifting with hydraulic systems [4], most studies do not focus on high-precision manipulation under tight tolerances. Although accurate manipulation has been extensively studied for industrial robotic arms [5], hydraulic cranes differ significantly in scale, compliance, actuation, and dynamics, limiting the direct transfer of existing methods.

In this work, we address the problem of accurate container lifting in urban recycling scenarios. We propose a residual reinforcement learning (RRL) framework that combines a reliable nominal Cartesian controller—responsible for trajectory tracking and swing suppression—with a learned residual policy that compensates for unmodeled dynamics and improves precision. This hybrid approach enables accurate and robust control without relying on end-to-end learning from scratch.

* qili@rptu.de



Figure 1. Simulated waste-container handling scenario.

This paper is organized as follows. Section 2 reviews related work. Section 3 presents the system, simulation, and the proposed RRL architecture. Section 4 reports experiments, and Section 5 provides ablations. Section 6 concludes and outlines future work.

2. Related Work

2.1. Hydraulic Machinery and Underactuated Loads

Model-based control of hydraulic manipulators has a long history, addressing nonlinear actuation and load-dependent dynamics [4, 6, 7]. Integrated autonomous systems such as HEAP demonstrate full-stack autonomy using classical controllers [8], but typically require detailed models and extensive tuning.

Reinforcement learning (RL) has recently been applied to hydraulic equipment, including excavation subtasks such as bucket filling and soil-adaptive excavation [9, 10], and scalable training paradigms for excavation [11–13]. For underactuated crane-like systems, learning-based control has been studied for multi-pendulum crane dynamics [14] and highly dynamic motions such as throwing and material handling [15, 16]. Forestry crane RL has also been reported [2, 17]. These efforts highlight strong adaptability, but they typically do not focus on precise hooking under tight tolerances with large-scale structural compliance.

2.2. Residual Reinforcement Learning

Residual reinforcement learning (RRL) augments a nominal controller with a learned residual policy to compensate for modeling errors and disturbances. Prior work shows rapid learning when residual policies refine stable impedance or demonstration-based controllers [18–20]. RRL is particularly appealing for large-scale systems where end-to-end RL can be sample-inefficient. Here, we apply RRL to combine trajectory tracking and anti-sway control with a residual policy that improves robustness and precision.

3. Methodology

3.1. System Description and Simulation Setup

We consider only the *container lifting* phase of the recycling workflow; transport, unloading, and release are omitted. All methods are developed and evaluated in Isaac Lab [21].

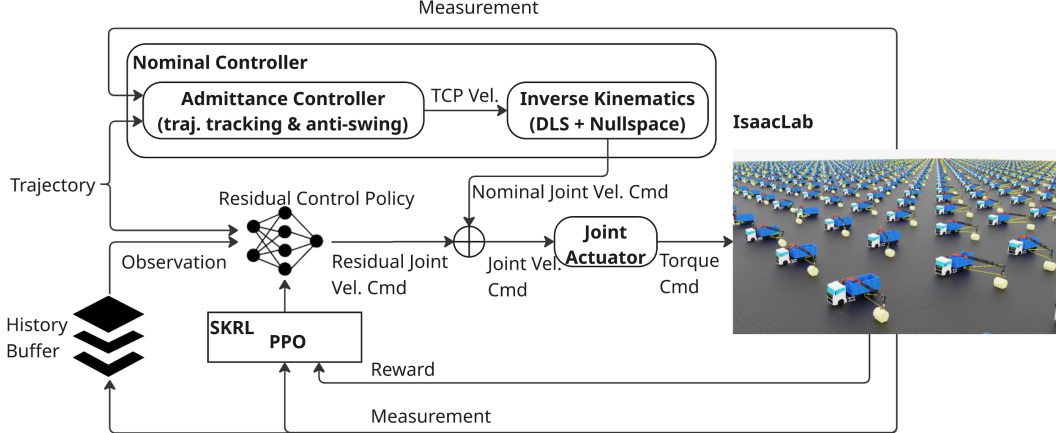


Figure 2. Overall control architecture. The nominal controller outputs ${}^{\text{nor}}u$ (TCP admittance + anti-swing + IK). A PPO-trained residual policy outputs ${}^{\text{res}}u$. The final joint-velocity command is $u = (1 - \lambda){}^{\text{nor}}u + \lambda{}^{\text{res}}u$ with error-dependent blending λ , and is applied to joint-level actuators.

The full system is summarized in Fig. 2. The simulated system is based on a modified loader crane mounted on a truck. The truck base is treated as rigid and fixed (no vehicle dynamics). The crane is a 7-DoF serial chain (3 revolute, 4 prismatic), with approximately 13 m outreach and a maximum lifting capacity of 7.1 t.

Hydraulic actuation and linkages are not explicitly modeled. Each joint is driven by a low-level PID controller whose gains are tuned and randomized to reproduce effects similar to structural compliance and bending that occur in large cranes. A discharge unit is attached at the crane tool center point (TCP) with two actuated joints (container rotation and hook open/close). Two *unactuated* revolute joints between the TCP and the discharge unit model underactuation; their motion is induced by gravity and crane accelerations, with small friction for damping (similar in spirit to pendulum modeling but captured directly by rigid-body simulation) [22]. The container is equipped with two hooking rings and has dimensions of roughly $1.6 \times 1.6 \times 1.8$ m, with a mass ranging from 100 kg to 700 kg.

The task requires accurate TCP positioning and swing suppression due to tight geometric tolerances between hooks and rings (Fig. 3). We assume an external perception system provides accurate 3D poses; perception uncertainty is not modeled.

3.2. Residual Reinforcement Learning

The task is simultaneous TCP trajectory tracking and swing suppression during hooking and lifting. A trusted Cartesian TCP trajectory is generated from the initial TCP and container poses and split into three segments (approach, horizontal alignment, lift), which introduced in Section 3.2.2. We adopt an RRL architecture (Fig. 2): a nominal controller provides stable baseline tracking and anti-swing behavior, while a residual policy compensates unmodeled dynamics.

3.2.1. Nominal Controller

The nominal controller operates in Cartesian space at the TCP and consists of: (i) an admittance controller for trajectory tracking, (ii) a pendulum-aware anti-swing acceleration term, and (iii) a damped least-squares inverse kinematics (IK) mapping to joint space.

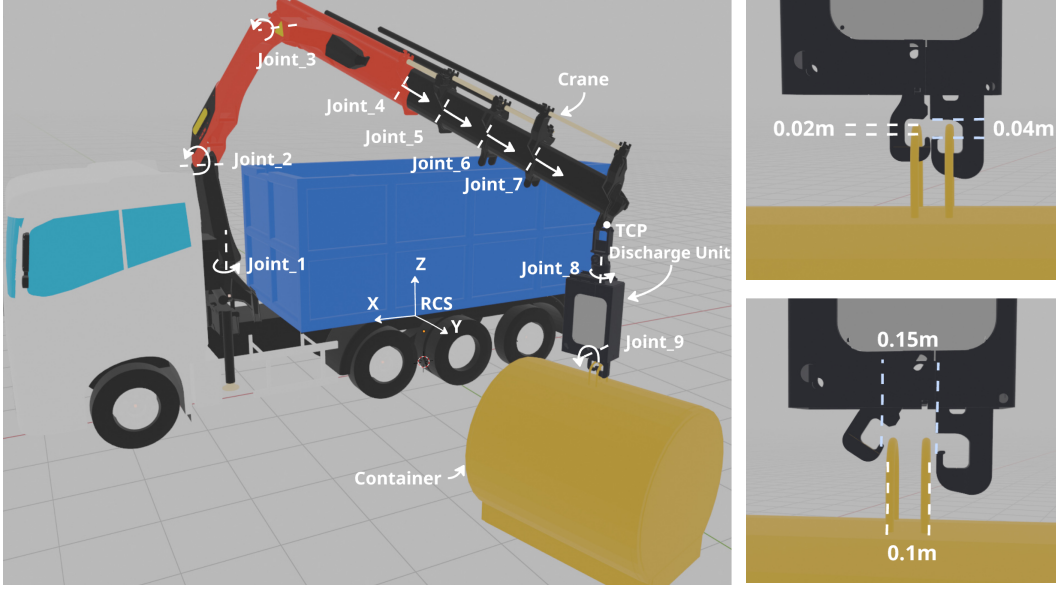


Figure 3. System overview. **Left:** crane kinematic model and task setup. **Right:** close-ups illustrating tight hook-ring tolerances.

Admittance Control with Anti-Swing Compensation. Let $x, v \in \mathbb{R}^3$ be TCP position/velocity and $x_{\text{ref}}, v_{\text{ref}}$ the reference. Define

$$e_p = x_{\text{ref}} - x, \quad e_v = v_{\text{ref}} - v, \quad e_i(t) = \int_0^t e_p(\tau) \, d\tau, \quad (3.1)$$

We construct a *virtual force* command

$$F_{\text{cmd}} = K_p e_p + K_v e_v + K_i e_i + M_d a_{xy}, \quad (3.2)$$

and integrate the admittance model

$$\begin{aligned} M_d \dot{v}_d + D_d v_d + K_d (x_d - x_{\text{ref}}) &= F_{\text{cmd}}, \\ v_d^{k+1} &= \text{sat}_{v_{\text{max}}}(v_d^k + \Delta t \dot{v}_d^k). \end{aligned} \quad (3.3)$$

Pendulum-Aware Anti-Swing Acceleration. For small swing angles, the discharge unit behaves approximately as

$$L \ddot{\theta} + g \theta \approx -a_{\text{TCP}}, \quad (3.4)$$

so horizontal TCP acceleration shapes sway [3, 23]. We command

$$a_{\text{TCP}} = k_\theta \theta + k_\omega \dot{\theta}, \quad (3.5)$$

yielding

$$\ddot{\theta} + \frac{k_\omega}{L} \dot{\theta} + \frac{g + k_\theta}{L} \theta = 0. \quad (3.6)$$

Matching to the standard second-order form

$$\ddot{\theta} + 2\zeta\omega_n \dot{\theta} + \omega_n^2 \theta = 0, \quad (3.7)$$

gives

$$k_\theta(L) = L\omega_n^2 - g, \quad k_\omega(L) = 2\zeta L\omega_n. \quad (3.8)$$

We apply this in both horizontal directions and filter swing estimates:

$$a_{xy} = w_s \begin{bmatrix} k_\theta \hat{\theta}_x + k_\omega \hat{\dot{\theta}}_x \\ k_\theta \hat{\theta}_y + k_\omega \hat{\dot{\theta}}_y \\ 0 \end{bmatrix}, \quad \hat{\theta}_{xy}^{k+1} = (1 - \alpha) \hat{\theta}_{xy}^k + \alpha \theta_{xy}^k, \quad \hat{\dot{\theta}}_{xy}^{k+1} = (1 - \alpha) \hat{\dot{\theta}}_{xy}^k + \alpha \dot{\theta}_{xy}^k. \quad (3.9)$$

Inverse Kinematics with Nullspace Optimization. The desired TCP velocity v_d is mapped to joint velocities using damped least-squares inverse kinematics augmented with a nullspace posture term:

$${}^{\text{nor}}u = J_\lambda^+ v_d + (I - J_\lambda^+ J) k_{\text{ns}}(q_c - q), \quad (3.10)$$

3.2.2. Learning the Residual Action

We follow the RRL formulation [24]. The residual policy outputs a correction a_r to improve precision under unmodeled dynamics. Since tight tolerances matter most during horizontal alignment, we apply the residual only in segment B (Fig. 4):

$$u = {}^{\text{nor}}u + {}^{\text{res}}u \text{ (segment B)}, \quad u = {}^{\text{nor}}u \text{ (segments A,C)}.$$

We use a trajectory-tube metric [16] to quantify adherence:

$$\delta_{\text{tube}} = \max \left(-\frac{r}{2}, r - \frac{\|(\mathbf{p}_{\text{tcp}} - \mathbf{p}_1) \times (\mathbf{p}_2 - \mathbf{p}_1)\|}{\|\mathbf{p}_2 - \mathbf{p}_1\|} \right), \quad (3.11)$$

where r is the tube radius and $\delta_{\text{tube}} > 0$ indicates the TCP remains inside the tube. The policy is trained with PPO using `skr1` [25] in Isaac Lab; the MLP has hidden sizes [128, 64, 32].

A. Observations and Actions

The policy input consists of an 78-dimensional observation vector formed by concatenating task-relevant geometric information, and previous action, proprioceptive states history over the last three time steps (Table 1). This history allows the policy to infer system dynamics and controller behavior. The tube distance δ_{tube} is included explicitly to inform the policy about trajectory adherence.

Observation	Notation	Dim.
Crane joint positions	$q_{1:7}^{t:t-2}$	21
Crane joint velocities	$\dot{q}_{1:7}^{t:t-2}$	21
Discharge unit joint positions	$q_{10:11}^{t:t-2}$	6
Discharge unit joint velocities	$\dot{q}_{10:11}^{t:t-2}$	6
Reference TCP points	$\text{rcs}_p^{t:t-2}$	9
Trajectory tube state	δ_{tube}	1
Previous nominal action	${}^{\text{nor}}u_{1:7}^{t-1}$	7
Previous residual action	${}^{\text{res}}u_{1:7}^{t-1}$	7

Table 1. Policy observations.

The residual action is a joint velocity correction for the crane:

$${}^{\text{res}}u = [\hat{q}_1, \dots, \hat{q}_7].$$

B. Reward and Termination

The reward at time step k is defined as a weighted sum of task-relevant components,

$$R_k = c_1 r_k^{\text{target-coarse}} + c_2 r_k^{\text{target-fine}} + c_3 r_k^{\text{tube}} + c_4 r_k^{\text{progress}} + c_7 r_k^{\text{oscillation}} + c_8 r_k^{\text{lifting}} + c_9 r_k^{\text{smooth}}, \quad (3.12)$$

where c_i are scalar weights.

The reward terms are computed using the TCP position p_k^{tcp} , discharge unit position p_k^d , container position p_k^c , and the current reference control point p_m^{ref} . The individual reward components are defined as

$$\begin{aligned} r_k^{\text{target-coarse}} &= -\frac{1}{\sigma} \max(0, d_{m,k} - \sigma), \\ r_k^{\text{target-fine}} &= 1 - \tanh\left(\frac{d_{m,k}}{\sigma}\right), \\ r_k^{\text{tube}} &= \mathbb{I}\left[\delta_{\text{tube},k} \geq 0 \wedge (p_k^{\text{tcp}} - p_{m-1}^{\text{ref}})^\top (p_m^{\text{ref}} - p_{m-1}^{\text{ref}}) \geq 0 \right. \\ &\quad \left. \wedge (p_k^{\text{tcp}} - p_m^{\text{ref}})^\top (p_m^{\text{ref}} - p_{m-1}^{\text{ref}}) \leq 0\right], \\ r_k^{\text{progress}} &= m/M, \\ r_k^{\text{oscillation}} &= 1 - \tanh\left(\frac{\arccos\left(\frac{\vec{v}_k^\top \mathbf{g}}{\|\vec{v}_k\|}\right) - \theta_{\max}}{\theta_{\max}}\right), \\ r_k^{\text{lifting}} &= \mathbb{I}(z_k^c > z_{\min}), \\ r_k^{\text{smooth}} &= -\sum_{i=1}^N (a_{k,i}^{\text{res}})^2, \end{aligned}$$

where

$$d_{m,k} = \|p_m^{\text{ref}} - p_k^{\text{tcp}}\|_2, \quad \vec{v}_k = p_k^d - p_k^{\text{tcp}},$$

The reward terms have complementary roles. The tracking rewards $r_k^{\text{target-coarse}}$ and $r_k^{\text{target-fine}}$ drive the TCP toward the current control point, with coarse shaping far from the target and fine shaping near it. r_k^{tube} encourages the TCP to stay within a tubular neighborhood of the active trajectory segment, while r_k^{progress} promotes forward motion along the path. $r_k^{\text{oscillation}}$ damps sway of the discharge unit relative to gravity, r_k^{lifting} rewards successful lift, and r_k^{smooth} penalizes large residual actions to encourage safe, smooth control.

Termination	Definition
Distance out of range (current control point)	$\left\ \mathbf{p}_k^{\text{ref}} - \mathbf{p}_k^{\text{pb}} \right\ _2 > d_{\max}$
TCP outside trajectory tube for n steps	$\sum_{j=1}^k \mathbb{I}(\delta_j^{\text{tube}} < 0) \geq n$
Discharge unit gravity misalignment	$\arccos\left(\frac{(p_k^d - p_k^{\text{tcp}})^\top \mathbf{g}}{\ p_k^d - p_k^{\text{tcp}}\ _2 \ \mathbf{g}\ _2}\right) > \theta_{\max}$

Table 2. Termination conditions.

To avoid unsafe or unrecoverable behaviors, episodes terminate early when (i) the TCP deviates too far from the current reference point, (ii) tube violations persist for n times, or (iii) the discharge unit tilt relative to gravity exceeds θ_{\max} . The termination event are list in Table 2.

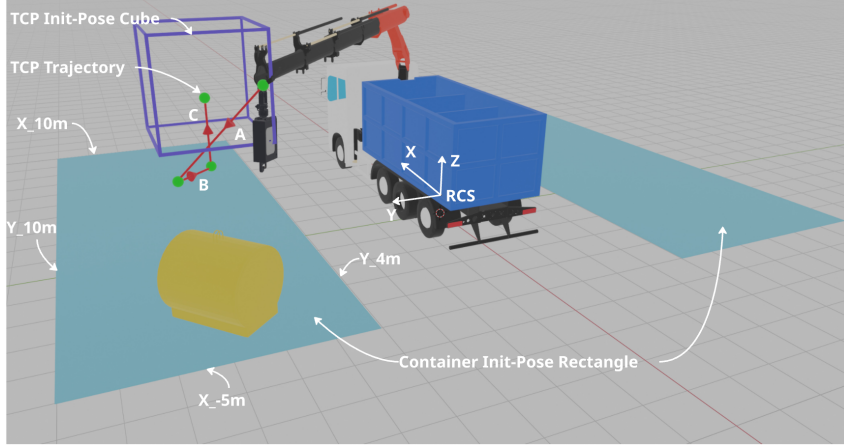


Figure 4. Randomized episode initialization: container spawned around the truck; TCP initialized in a cube above the container. TCP trajectory consists 3 segments (A, B, C) is generated according container and TCP position.

C. Episode Initialization and Domain Randomization

Episode Initialization. At reset, the container pose is uniformly sampled within a bounded horizontal workspace around the truck (fixed height for ground contact) and its yaw is randomized within preset limits. Conditioned on the sampled container pose, the crane TCP is initialized by uniformly sampling a position in a cubic region above the container (Fig. 4); the corresponding initial joint configuration is computed via inverse kinematics. A reference TCP trajectory is then generated as a spline between the initial and target poses and discretized into a fixed number of control points that are provided sequentially as tracking targets.

Domain Randomization. To reduce sensitivity to modeling errors, we apply domain randomization at episode reset. We perturb container mass and center of mass to vary payload and pendulum dynamics, randomize actuator stiffness and damping to capture uncertainties in joint behavior, and randomize friction parameters of the unactuated discharge-unit joints. Finally, we scale the nominal admittance-controller gains to expose the residual policy to a range of baseline controller behaviors.

4. Experiments

All experiments are conducted in simulation using Isaac Lab. The goal is to evaluate the proposed residual reinforcement learning (RRL) framework on the container lifting task with a large-scale loader crane and an underactuated discharge unit. Performance is evaluated along four aspects: (i) TCP trajectory tracking accuracy, (ii) satisfaction of the trajectory tube constraint, (iii) swing suppression of the discharge unit, and (iv) robustness to parameter variations. For unbiased evaluation, test episodes are evenly sampled from container initial positions on the left and right sides of the truck workspace (Fig. 4), and all metrics are aggregated over these symmetric configurations.

4.1. Trajectory Tracking and Tube Constraint

Figure 5(a) illustrates a representative reference TCP trajectory and the corresponding executed trajectory, while Fig. 5(b–g) shows the crane motion sequence. Tracking accuracy is quantified by the Euclidean distance between the executed TCP and the reference trajectory.

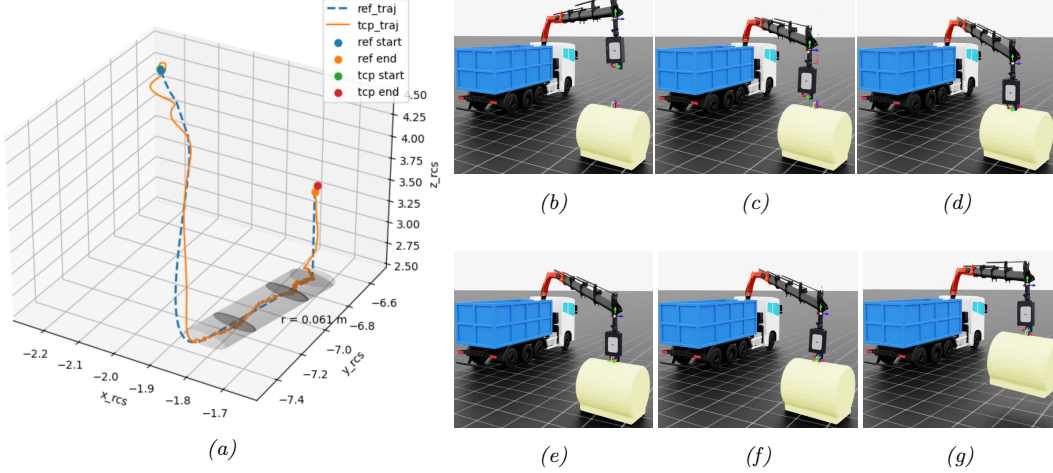


Figure 5. Representative lifting episode: (a) reference vs. executed TCP trajectory; (b–g) motion sequence.

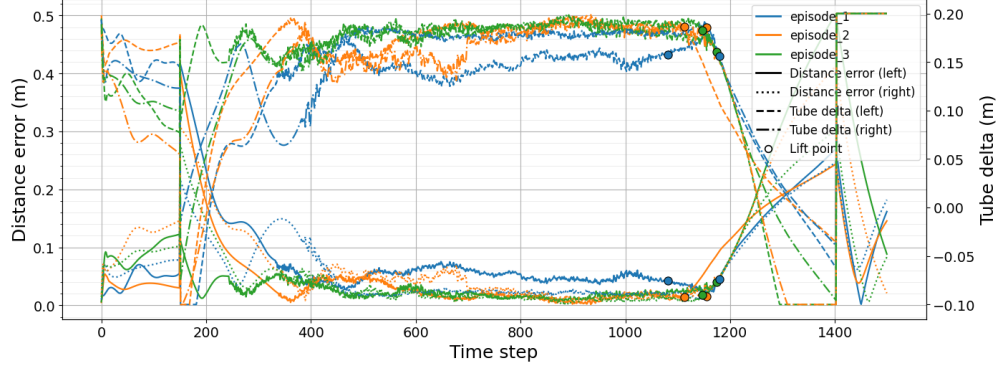


Figure 6. TCP tracking error and trajectory tube delta for representative episodes.

To analyze accuracy relative to the trajectory tube constraint, we record both the TCP tracking error and the tube delta (Eq. 3.11) over time. Figure 6 reports results from three representative episodes on each side of the workspace. A larger tube delta corresponds to the TCP remaining closer to the reference trajectory and is consistently associated with lower tracking error. At the lifting instant, the TCP tracking error remains below 0.04 m, which is sufficient to satisfy the tight geometric tolerances required for reliable container hooking.

4.2. Swing Suppression

Figure 7 shows the swing angle of the discharge unit relative to gravity for the same evaluation episodes. Initial oscillations induced by crane motion are effectively damped over time by the nominal controller and residual policy. At the lifting point, four out of six episodes exhibit swing angles below 2.5°, while all episodes remain within acceptable limits. Compared to peak initial swings of up to 17.5°, this demonstrates substantial reduction in oscillation amplitude prior to lifting.

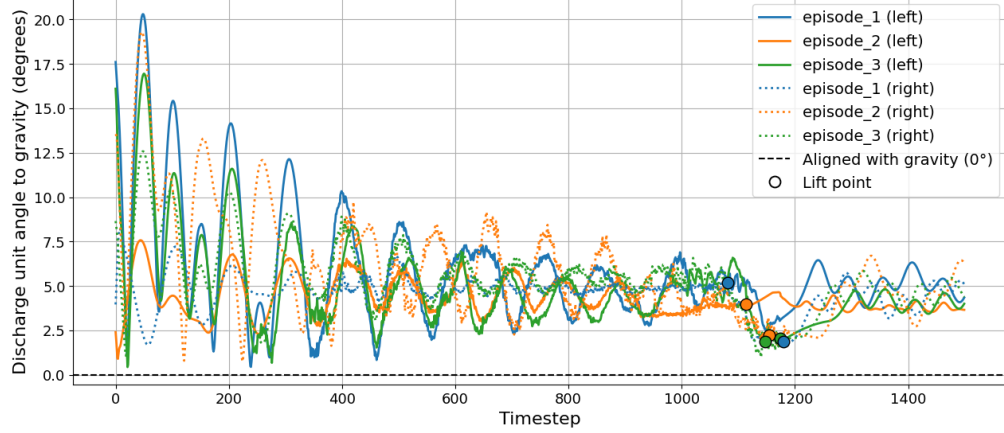


Figure 7. Swing angle of the discharge unit relative to gravity over time.

Randomization	Tracking Error(m)				Swing Angle(deg)			
	Mean		Mean		Mean		Mean	
	Std	[700,1200]	Std	[700,1200]	Std	[700,1200]	Std	[700,1200]
scale_0.1_0.49	0.147	0.087	0.103	0.127	3.096	3.555	6.271	5.166
scale_0.5_1.5	0.073	0.019	0.026	0.015	2.046	1.316	4.016	1.378
scale_1.51_2.0	0.049	0.008	0.014	0.004	2.584	1.641	4.544	1.414

Randomization	Tube Delta(m)				Success Rate			
	Mean		Mean		z ^c > 0.5 m			
	Std	[700,1200]	Std	[700,1200]				
scale_0.1_0.49	0.089	0.050	0.114	0.077	47.3%			
scale_0.5_1.5	0.140	0.015	0.174	0.015	90.0%			
scale_1.51_2.0	0.158	0.008	0.187	0.004	92.3%			

Table 3. Performance metrics aggregated over three randomization groups.

4.3. Robustness to Parameter Variations

Robustness is evaluated under parameter settings that differ from those used during training. During training, actuator gains, passive joint damping, and nominal controller gains are randomized within scale of [0.5, 1.5]. For evaluation, three disjoint ranges are considered: (i) scale_0.1–0.49 (softer system), (ii) scale_0.5–1.5 (training range), (iii) scale_1.51–2.0 (stiffer system). Each setting is evaluated over 300 episodes (150 left, 150 right). The results are summarized in Table 3.

The stiff configuration (scale_1.51–2.0) achieves the best tracking accuracy and highest success rate, as increased stiffness reduces crane bending and improves trajectory following. However, swing angles are slightly larger due to altered crane dynamics. The soft configuration (scale_0.1–0.49) is the most challenging, resulting in larger tracking errors and reduced tube adherence due to increased compliance. Nevertheless, even in this case the method achieves a 47.3% lifting success rate, with mean swing angles at lift around 3°, which remains acceptable given the length of the discharge unit.

Models			Tracking Error(m)				Swing Angle(deg)			
Nominal Controller		RRL	Mean	Std	Mean	Std	Mean	Std	Mean	Std
Traj. Tracking		Anti-Swing	[700,1200)				[700,1200)			
•	—	—	0.100	0.025	0.089	0.030	3.318	3.100	7.792	2.819
•	—	•	0.071	0.018	0.021	0.014	2.361	1.520	4.355	1.533
•	•	—	0.105	0.031	0.098	0.039	2.719	2.353	6.545	2.880
•	•	•	0.073	0.021	0.027	0.014	2.090	1.440	4.033	1.303

Models			Tube Delta(m)				Success Rate			
Nominal Controller		RRL	Mean	Std	Mean	Std	$z^c > 0.5$ m			
Traj. Tracking		Anti-Swing	[700,1200)				[700,1200)			
•	—	—	0.110	0.023	0.111	0.030	57.3%			
•	—	•	0.140	0.014	0.179	0.014	88.3%			
•	•	—	0.105	0.027	0.103	0.039	71.3%			
•	•	•	0.139	0.016	0.173	0.014	91.7%			

Table 4. Performance metrics aggregated over 4 different models.

Overall, these results demonstrate that the proposed RRL framework significantly improves trajectory tracking, swing suppression, and robustness compared to the nominal controller alone, particularly under challenging dynamic conditions.

5. Ablation Studies

To assess the contribution of each component in the proposed control architecture (Fig. 2), we perform an ablation study on four controller variants: (i) nominal controller with trajectory tracking only, (ii) trajectory tracking with residual reinforcement learning (RRL), (iii) trajectory tracking with anti-swing control, and (iv) trajectory tracking with anti-swing control and RRL. For configurations involving RRL, the residual policy is retrained accordingly. Each variant is evaluated over 300 episodes (150 left, 150 right), and the results are summarized in Table 4.

Anti-Swing Control. Without RRL, adding the anti-swing module improves the success rate from 57.3% to 71.3%, demonstrating its effectiveness in reducing pendulum oscillations and improving task reliability.

Residual Reinforcement Learning. Introducing RRL significantly boosts performance in both cases. Without anti-swing, RRL increases the success rate from 57.3% to 88.3%, showing its ability to compensate for unmodeled dynamics. When anti-swing is present, RRL further improves the success rate from 71.3% to 91.7%, indicating complementary benefits.

Tracking and Swing Performance. TCP tracking error and tube delta vary only slightly across configurations, confirming that trajectory tracking is mainly handled by the nominal controller, with RRL providing a modest refinement. In contrast, swing angle metrics show substantial differences: anti-swing control significantly reduces oscillations, and RRL further lowers swing amplitudes, achieving the best overall performance when both are combined.

In summary, the ablation study confirms that the anti-swing module provides an effective model-based foundation, while the residual reinforcement learning policy substantially enhances robustness and success by compensating for unmodeled effects.

6. Conclusion and Future Work

This work presented a residual reinforcement learning approach for accurate container lifting with a large-scale hydraulic loader crane and an underactuated discharge unit. By combining a nominal admittance controller with pendulum-aware anti-swing control and a learned residual policy, the proposed method achieves improved tracking accuracy, effective swing suppression, and robust performance under parameter variations in simulation.

Several directions are planned for future research. First, we will extend the framework to explicitly account for hydraulic dynamics, enabling adaptation of the residual policy to real actuator behavior. Second, more realistic simulation of hydraulic systems will be incorporated during training to reduce the sim-to-real gap. Finally, we plan to validate the proposed method on a real loader crane platform and investigate additional domain adaptation techniques to further improve transfer from simulation to real-world deployment.

Acknowledgements

This work was carried out within a publicly funded project of the Commercial Vehicle Cluster (CVC), Rheinland-Pfalz, Germany, in collaboration with Palfinger AG. Palfinger AG provided the CAD model of the loader crane and the discharge unit used in this research.

References

- [1] R. L. Johns, M. Wermelinger, R. Mascaro, D. Jud, I. Hurkxkens, L. Vasey, M. Chli, F. Gramazio, M. Kohler, and M. Hutter. “A framework for robotic excavation and dry stone construction using on-site materials”. In: *Science Robotics* 8.84 (2023), eabp9758. DOI: [10.1126/scirobotics.abp9758](https://doi.org/10.1126/scirobotics.abp9758). URL: <https://www.science.org/doi/10.1126/scirobotics.abp9758>.
- [2] J. Andersson, K. Bodin, D. Lindmark, M. Servin, and E. Wallin. *Reinforcement Learning Control of a Forestry Crane Manipulator*. 2021. arXiv: [2103.02315 \[cs.R0\]](https://arxiv.org/abs/2103.02315). URL: <https://arxiv.org/abs/2103.02315>.
- [3] Y.-G. Sun, H.-Y. Qiang, J. Xu, and D.-S. Dong. “The Nonlinear Dynamics and Anti-Sway Tracking Control for Offshore Container Crane on a Mobile Harbor”. In: *Journal of Marine Science and Technology* 25.6 (2017), Article 5. DOI: [10.6119/JMST-017-1226-05](https://doi.org/10.6119/JMST-017-1226-05). URL: <https://jmstt.ntou.edu.tw/journal/vol25/iss6/5>.
- [4] Q. Ha, M. Santos, Q. Nguyen, D. Rye, and H. Durrant-Whyte. “Robotic excavation in construction automation”. In: *IEEE Robotics & Automation Magazine* 9.1 (2002), pp. 20–28. DOI: [10.1109/100.993151](https://doi.org/10.1109/100.993151).
- [5] L. Han, J. Mao, C. Zhang, R. W. Kay, R. C. Richardson, and C. Zhou. “A systematic trajectory tracking framework for robot manipulators: An observer-based nonsmooth control approach”. In: *IEEE Transactions on Industrial Electronics* 71.9 (2023), pp. 11104–11114.
- [6] P. H. Chang and S.-J. Lee. “A straight-line motion tracking control of hydraulic excavator system”. In: *Mechatronics* 12.1 (2002), pp. 119–138. ISSN: 0957-4158. DOI: [https://doi.org/10.1016/S0957-4158\(01\)00014-9](https://doi.org/10.1016/S0957-4158(01)00014-9). URL: <https://www.sciencedirect.com/science/article/pii/S0957415801000149>.
- [7] J. Mattila, J. Koivumäki, D. G. Caldwell, and C. Semini. “A Survey on Control of Hydraulic Robotic Manipulators With Projection to Future Trends”. In: *IEEE/ASME Transactions on Mechatronics* 22.2 (2017), pp. 669–680. DOI: [10.1109/TMECH.2017.2668604](https://doi.org/10.1109/TMECH.2017.2668604).
- [8] D. Jud, S. Kerscher, M. Wermelinger, E. Jelavic, P. Egli, P. Leemann, G. Hottiger, and M. Hutter. “HEAP - The autonomous walking excavator”. In: *Automation in Construction* 129 (Sept. 2021), p. 103783. ISSN: 0926-5805. DOI: [10.1016/j.autcon.2021.103783](https://doi.org/10.1016/j.autcon.2021.103783). URL: [http://dx.doi.org/10.1016/j.autcon.2021.103783](https://dx.doi.org/10.1016/j.autcon.2021.103783).
- [9] P. Egli, L. Terenzi, and M. Hutter. “Reinforcement Learning-Based Bucket Filling for Autonomous Excavation”. In: *IEEE Transactions on Field Robotics* 1 (2024), pp. 170–191. DOI: [10.1109/TFR.2024.3432508](https://doi.org/10.1109/TFR.2024.3432508).

[10] P. Egli, D. Gaschen, S. Kerscher, D. Jud, and M. Hutter. “Soil-Adaptive Excavation Using Reinforcement Learning”. In: *IEEE Robotics and Automation Letters* 7.4 (2022), pp. 9778–9785. doi: [10.1109/LRA.2022.3189834](https://doi.org/10.1109/LRA.2022.3189834).

[11] Y. Zhai, L. Terenzi, P. Frey, D. G. Soto, P. Egli, and M. Hutter. *ExT: Towards Scalable Autonomous Excavation via Large-Scale Multi-Task Pretraining and Fine-Tuning*. 2025. arXiv: [2509.14992 \[cs.R0\]](https://arxiv.org/abs/2509.14992). URL: <https://arxiv.org/abs/2509.14992>.

[12] J. Gruetter, L. Terenzi, P. Egli, and M. Hutter. *Towards Learning Boulder Excavation with Hydraulic Excavators*. 2025. arXiv: [2509.17683 \[cs.R0\]](https://arxiv.org/abs/2509.17683). URL: <https://arxiv.org/abs/2509.17683>.

[13] P. Egli and M. Hutter. “Towards RL-Based Hydraulic Excavator Automation”. In: *2020 IEEE/RSJ International Conference on Intelligent Robots and Systems (IROS)*. 2020, pp. 2692–2697. doi: [10.1109/IROS45743.2020.9341598](https://doi.org/10.1109/IROS45743.2020.9341598).

[14] Q. Wu, N. Sun, T. Yang, and Y. Fang. “Deep Reinforcement Learning-Based Control for Asynchronous Motor-Actuated Triple Pendulum Crane Systems With Distributed Mass Payloads”. In: *IEEE Transactions on Industrial Electronics* 71.2 (2024), pp. 1853–1862. doi: [10.1109/TIE.2023.3262891](https://doi.org/10.1109/TIE.2023.3262891).

[15] L. Werner, F. Nan, P. Eyschen, F. A. Spinelli, H. Yang, and M. Hutter. *Dynamic Throwing with Robotic Material Handling Machines*. 2024. arXiv: [2405.19001 \[cs.R0\]](https://arxiv.org/abs/2405.19001). URL: <https://arxiv.org/abs/2405.19001>.

[16] F. A. Spinelli, Y. Zhai, F. Nan, P. Egli, J. Nubert, T. Bleumer, L. Miller, F. Hofmann, and M. Hutter. *Large Scale Robotic Material Handling: Learning, Planning, and Control*. 2025. arXiv: [2508.09003 \[cs.R0\]](https://arxiv.org/abs/2508.09003). URL: <https://arxiv.org/abs/2508.09003>.

[17] E. Wallin, V. Wiberg, and M. Servin. *Multi-log grasping using reinforcement learning and virtual visual servoing*. 2024. arXiv: [2309.02997 \[cs.R0\]](https://arxiv.org/abs/2309.02997). URL: <https://arxiv.org/abs/2309.02997>.

[18] P. Kulkarni, J. Kober, R. Babuška, and C. Della Santina. “Learning Assembly Tasks in a Few Minutes by Combining Impedance Control and Residual Recurrent Reinforcement Learning”. In: *Advanced Intelligent Systems* 4.1 (2022), p. 2100095. doi: <https://doi.org/10.1002/aisy.202100095>. eprint: <https://advanced.onlinelibrary.wiley.com/doi/pdf/10.1002/aisy.202100095>. URL: <https://advanced.onlinelibrary.wiley.com/doi/abs/10.1002/aisy.202100095>.

[19] M. Alakuijala, G. Dulac-Arnold, J. Mairal, J. Ponce, and C. Schmid. *Residual Reinforcement Learning from Demonstrations*. 2021. arXiv: [2106.08050 \[cs.LG\]](https://arxiv.org/abs/2106.08050). URL: <https://arxiv.org/abs/2106.08050>.

[20] L. Ankile, Z. Jiang, R. Duan, G. Shi, P. Abbeel, and A. Nagabandi. *Residual Off-Policy RL for Finetuning Behavior Cloning Policies*. 2025. arXiv: [2509.19301 \[cs.R0\]](https://arxiv.org/abs/2509.19301). URL: <https://arxiv.org/abs/2509.19301>.

[21] NVIDIA et al. *Isaac Lab: A GPU-Accelerated Simulation Framework for Multi-Modal Robot Learning*. 2025. arXiv: [2511.04831 \[cs.R0\]](https://arxiv.org/abs/2511.04831). URL: <https://arxiv.org/abs/2511.04831>.

[22] F. A. Spinelli, P. Egli, J. Nubert, F. Nan, T. Bleumer, P. Goegler, S. Brockes, F. Hofmann, and M. Hutter. “Reinforcement Learning Control for Autonomous Hydraulic Material Handling Machines with Underactuated Tools”. In: *2024 IEEE/RSJ International Conference on Intelligent Robots and Systems (IROS)*. IEEE, Oct. 2024, pp. 12694–12701. doi: [10.1109/iros58592.2024.10802199](https://doi.org/10.1109/iros58592.2024.10802199). URL: [http://dx.doi.org/10.1109/IROS58592.2024.10802199](https://dx.doi.org/10.1109/IROS58592.2024.10802199).

[23] H.-y. Qiang, Y.-g. Sun, J.-c. Lyu, and D.-s. Dong. “Anti-Sway and Positioning Adaptive Control of a Double-Pendulum Effect Crane System With Neural Network Compensation”. In: *Frontiers in Robotics and AI* Volume 8 - 2021 (2021). ISSN: 2296-9144. doi: [10.3389/frobt.2021.639734](https://doi.org/10.3389/frobt.2021.639734). URL: <https://www.frontiersin.org/journals/robotics-and-ai/articles/10.3389/frobt.2021.639734>.

[24] T. Johannink, S. Bahl, A. Nair, J. Luo, A. Kumar, M. Loskyll, J. Aparicio Ojea, E. Solowjow, and S. Levine. *Residual Reinforcement Learning for Robot Control*. 2018. arXiv: [1812.03201 \[cs.R0\]](https://arxiv.org/abs/1812.03201). URL: <https://arxiv.org/abs/1812.03201>.

[25] A. Serrano-Muñoz, D. Chrysostomou, S. Bøgh, and N. Arana-Arexolaleiba. “skrl: Modular and Flexible Library for Reinforcement Learning”. In: *Journal of Machine Learning Research* 24.254 (2023), pp. 1–9. URL: <http://jmlr.org/papers/v24/23-0112.html>.